Cerenkov Luminescence Tomography of Aminopeptidase N (APN/CD13) Expression in Mice Bearing HT1080 Tumors

Zhenhua Hu, Weidong Yang,* Xiaowei Ma, Wenhui Ma, Xiaochao Qu, Jimin Liang, Jing Wang, and Jie Tian*

Abstract

In vivo imaging of aminopeptidase N (APN/CD13) expression is crucial for the early detection of cancer. This study attempted to show that APN/CD13 expression can be imaged and quantified with novel Cerenkov luminescence tomography (CLT). Na[131]I with various activities was placed at different depths in a tissue-mimicking phantom, and various porcine tissues and luminescent images were acquired. The binding of ^{131}I-NGR with human fibrosarcoma HT1080 and human colon cancer HT-29 cells was detected with Cerenkov luminescence imaging (CLI). Nude mice bearing HT-1080 tumors were imaged after injection with ^{131}I-NGR using both planar and tomographic CLI methods. The penetration depth increased with ascending activity of Na[131]I. There was a robust linear correlation between the optical signal intensity and the HT1080 cell numbers ($r^2 = .9691$), as well as the activity ($r^2 = .9860$). The three-dimensional visualization CLT results clearly showed that ^{131}I-NGR uptake in tumor tissues represented a high expression of the APN/CD13 receptor. CLT also allowed quantifying ^{131}I-NGR uptake in tumor tissues showing an average activity of $0.1388 \pm 4.6788E-6$ MBq in tumor tissues. Our study indicated that ^{131}I-NGR combined with CLT allowed us to image and quantify tumor-associated APN/CD13 expression noninvasively. The promising CLT technique could be potentially used for sensitively evaluating tumor angiogenesis in vivo.

IN 1971, FOLKMAN postulated that the growth and metastasis of tumors were determined by angiogenesis.[1] Tumors cannot grow beyond the size of 1 to 2 mm without the formation of neovasculature to provide oxygen and nutrients.[2] Aminopeptidase N (APN/CD13) is a Zn^{2+}-dependent membrane-bound ectopeptidase that preferentially degrades proteins and peptides with an N-terminal neutral amino acid.[3] The transmembrane molecule CD13 is expressed on endothelial cells and has been demonstrated to be associated with cancer invasion, metastasis, and angiogenesis, indicating a suitable target for anticancer therapy.[3]

In vivo imaging of APN/CD13 expression is crucial for the early detection of cancer. The asparagine-glycine-arginine (NGR)-containing peptide selected by phage display can specifically target tumor vasculature.[4] Recognizing the APN/CD13 receptor on the membrane of tumor cells, the peptide can be further internalized into the cytoplasm via the endosomal pathway.[4] Hence, NGR can serve as an ideal molecular probe for tumor imaging by being conjugated with fluorescent materials or a radionuclide.[4,5] However, nuclear imaging is very expensive and has low throughput and low resolution. Fluorescence-mediated tomography (FMT) has the problem of inherent background noise and probe toxicity. Therefore, existing nuclear imaging and optical imaging methods are not optimal for imaging APN/CD13 expression.

Recently, Cerenkov radiation–based luminescence imaging (CLI) has emerged,[6–18] which can image the radionuclide with high-energy particles with an optical imaging instrument. The novel technique can overcome the limitations of existing imaging methods. Cerenkov radiation is a well-known phenomenon in which visible and near-infrared photons are emitted when a charged and high-energy particle travels in a dielectric medium at a velocity faster than the speed of light. The emitted visible and near-infrared photons from the radionuclide can be detected

Authors who contributed equally to this work.

From the School of Life Sciences and Technology, Xidian University, Xi'an, China; Department of Nuclear Medicine, Xijing Hospital, Fourth Military Medical University, Xi'an, China; and Institute of Automation, Chinese Academy of Sciences, Beijing, China.

Address reprint requests to: Jimin Liang, PhD, School of Life Sciences and Technology, Xidian University, Xi'an 710071, China; e-mail: jimleung@mail.xidian.edu.cn; Jing Wang, PhD, MD, Department of Nuclear Medicine, Xijing Hospital, Fourth Military Medical University, Xi'an 710032, China; e-mail: wangjing@fmmu.edu.cn; or Jie Tian, PhD, Institute of Automation, Chinese Academy of Sciences, Beijing 100190, China; e-mail: tian@ieee.org.

DECKERx

using a highly sensitive charge-coupled device (CCD) camera. Recently, CLI has become a motivating topic.[6–18] Robertson and colleagues first performed CLI on mice using positron-emitting radionuclide tracers.[6] Liu and colleagues successfully demonstrated that a variety of radionuclide-labeled probes can be used for CLI in small animals.[8]

Currently, CLI is mainly used in two-dimensional (2D) imaging.[6–15] Nevertheless, 2D planar imaging cannot provide three-dimensional (3D) biodistribution and quantification information of the radionuclide-labeled probe in living small animals. Li and colleagues presented 3D Cerenkov lumines-cence tomography (CLT) based on a homogeneous mouse model using ^{18}F-fluorodeoxyglucose (^{18}F-FDG).[16] However, the assumption of a homogeneous optical property back-ground will lead to inaccurate source reconstruction.[19,20] In our previous study, we performed in vivo 3D CLT based on a heterogeneous mouse model with an implanted Na[131]I radioactive source.[17] Our results showed that the reconstruc-tion based on a heterogeneous mouse model was more accurate in localization than using the homogeneous one.

In the current study, we employed the CLT method to image and quantify APN/CD13 expression. It was necessary to acquire the Cerenkov optical signal of the mice bearing HT1080 tumors injected with ^{131}I-NGR for the reconstruc-tion of ^{131}I-NGR uptake in the tumor tissues. Whether the Cerenkov luminescence signal could be detected by the CCD camera was influenced by many factors, such as the depth, affinity, and specificity of ^{131}I-NGR and the variety of biologic tissues. Therefore, we first investigated the penetration of Cerenkov luminescence emitted from Na[131]I through ex vivo experiments using the tissue-mimicking phantom and various porcine tissues. We then labeled NGR peptide with ^{131}I and measured a specific tumor-targeted ^{131}I-NGR conjugate on an HT1080 fibro-sarcoma and HT-29 colon cancer cell in the in vitro cell experiment. Next, we conducted in vitro CLI of ^{131}I-NGR uptake in two cell lines. Finally, we performed CLT of APN/CD13 expression in mice bearing HT1080 tumors. The activity of ^{131}I-NGR uptake in the tumor tissues was reconstructed based on the semiquantitative Cerenkov radiation spectral characteristic–based Cerenkov lumines-cent source reconstruction method.

Materials and Methods

Penetration of Luminescence Emitted from Na[131]I in the Tissue-Mimicking Phantoms

Cubic phantoms ($n = 5$) were used in the investigation of the penetration depth of CLI (Figure 1A). The tissue-mimicking
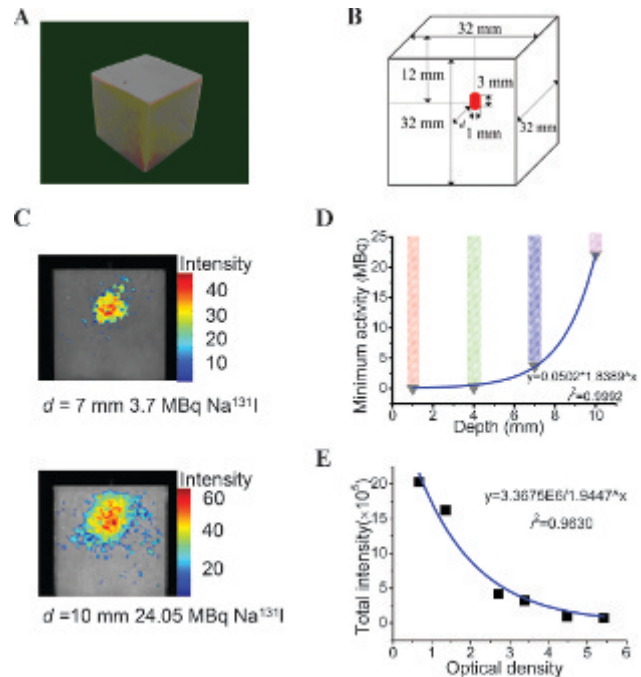

Figure 1. Phantom experiment. Radionuclide-labeled probe Na[131]I with various activities was placed in the hole of the tissue-mimicking phantoms ($n = 5$), and luminescent images were acquired. The probe depth was 1, 4, 7, 10, and 13 mm, respectively. *A* and *B* are the photograph and schematic diagram of the tissue-mimicking cubic phantoms, respectively. We acquired optical signals emitted from the Na[131]I with the activity of 3.7 MBq at a depth of 7 mm and 24.05 MBq at a depth of 10 mm (C). The approximate minimal activity exponentially increased with an increase in Na[131]I depth (D). Optical intensity decreased with increasing optical density (y = 3.3675E6/1.9447^x, r^2 = .9630) (E).

phantoms were made from nylon, which simulated the mouse lungs measuring 32 mm in the lateral dimension. A small hole with a 1 mm diameter and a 12 mm depth from the top surface of each phantom was drilled to place the radioactive source (Figure 1B). The distance, *d*, between the center of the hole and the front surface of the phantom was 1, 4, 7, 10, and 13 mm, respectively. The refractory index for the phantom was 1.53. In the phantom experiment, radionuclide-labeled Na[131]I probes with various activities ($n = 10$) were injected at the bottom of the glass capillaries as the radioactive sources. The capillaries were made of glass. Each glass capillary was then placed into the hole of the phantoms, and luminescent images were acquired one by one. For each glass capillary, the experiment was performed more than three times. The dimensions of the glass capillaries were approximately 2 mm in diameter and 15 mm in height. The activities of Na[131]I were 0.0185, 0.037, 0.074, 0.185, 1.48, 2.96, 3.7, 11.1, 18.5, and 24.05 MBq, respectively. The height was approximately 3 mm.

Furthermore, we investigated the relationship between optical intensity and optical density using the cubic phantoms ($n = 6$). The phantoms were made from nylon, had the same refractive index of 1.53, and measured 32 mm in the lateral dimension (see Figure 1A). The distance, d, between the center of the hole and the front surface of the phantom was 1, 2, 4, 5, 7, and 8 mm, respectively. Na^{131}I with the activity of 7.4 MBq was injected in the bottom of a glass capillary and then placed into the hole of the phantoms, and luminescent images were acquired one by one.

Penetration of Luminescence Emitted from Na^{131}I in Various Porcine Tissues

Considering that the phantoms were not real biologic tissues, we further investigated the penetration depth of CLI using porcine tissues, including kidneys, fat, heart, and muscle (Figure 2A). The just-butchered porcine tissues were frozen at $-20°C$ and then cut into slices of various thicknesses using a microtome. The dimensions of the slices were approximately 10 mm in width and 70 mm in length. The thicknesses of the porcine tissues were from 1 to 8 mm, with a 1 mm interval. The linear radioactive sources were made of glass capillaries ($n = 4$) filled with Na^{131}I. The dimensions of the glass capillaries were approximately 1 mm in diameter and 50 mm in length. The activities of Na^{131}I were 0.4625, 0.925, 1.85, and 3.70 MBq, respectively. The volume of Na^{131}I was 50 μL. The capillaries were placed under the porcine tissues of various thicknesses, including 1, 2, 3, 4, 5, 6, 7, and 8 mm,

and then luminescent images were acquired. The experiment was conducted three times.

^{131}I Radiolabeling of NGR

NGR-containing peptide [cyclo-(Cys-Asn-Gly-Arg-Cys) Gly-Gly-Tyr] was purchased from the Jier Biochemical Company (Shanghai, China). All chemicals were used as purchased without further purification. Peptides were dissolved in a phosphate-buffered saline (PBS) buffer (0.1 N, pH 7.4) and frozen at $-20°C$. NGR peptide was labeled with ^{131}I via the iodogen method. Briefly, 37 MBq of ^{131}I (Beijing Atom High Tech, Beijing, China), 20 μg of NGR peptide, and 100 μL of 0.2 M phosphate buffer (pH 7.4) were added to the vial coated with 50 μg Iodogen (Sigma-Aldrich, St. Louis, MO). After reacting for 7 to 10 minutes at room temperature, the labeling yield of ^{131}I-NGR was measured by instant thin-layer chromatography (ethanol:water:ammonia water = 2:1:5 as the mobile phase) on a radio-thin-layer mini scanner (Bioscan, Washington, DC). The stability of ^{131}I-NGR was studied at room temperature for 4, 8, 12, and 24 hours.

Cell Culture

Human fibrosarcoma HT1080 and human colon cancer HT-29 cells were cultured in high-glucose Dulbecco's Modified Eagle's Medium (DMEM). Cells were grown routinely in a monolayer culture at $37°C$ in a 5% CO_2 humidified air atmosphere. APN/CD13-specific antibody H300 for immunofluorescence was from Santa Cruz Biotechnology (Santa Cruz, CA).
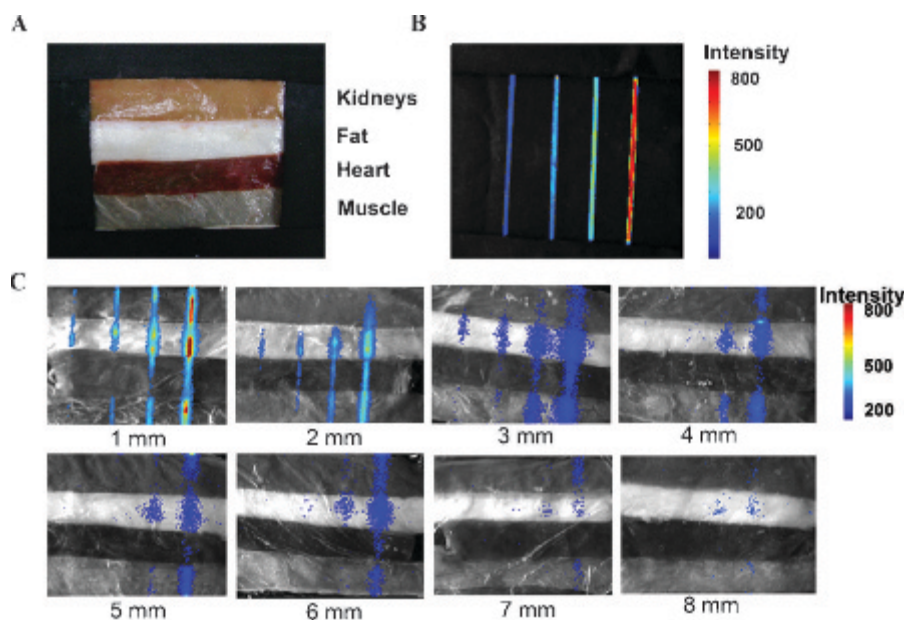

Figure 2. Penetration depth experiment with porcine tissues. The linear radioactive sources were made of glass capillaries ($n = 4$) filled with Na^{131}I. The activities of Na^{131}I were 0.4625, 0.925, 1.85, and 3.70 MBq, respectively. They were put in position at different depths in the porcine tissues, and luminescent images were acquired. *A*, The porcine tissues, including kidneys, fat, heart, and muscle. *B*, The linear radioactive sources Na^{131}I ($n = 4$) were acquired for the luminescent images. *C*, The linear radioactive sources of Na^{131}I ($n = 4$) at different depths in the porcine tissues acquired for the luminescent images. The depths of the linear radioactive sources were 1, 2, 3, 4, 5, 6, 7, and 8 mm, respectively.

Immunofluorescence

To investigate cellular expression of the CD13 receptor, HT1080 and HT-29 cells were plated into 24-well plates at a density of 50,000 cells/well. Cells were fixed in 4% (m/v) paraformaldehyde for 10 minutes after overnight incubation at 37°C. Cells were then washed with PBS saline, blocked in normal goat serum (1%), and then incubated with an anti-CD13 polyclonal antibody H300 (Santa Cruz Biotechnology) overnight at 4°C. Fluorescein isothiocyanate goat antirabbit IgG (Invitrogen, Carlsbad, CA) was used as the secondary antibody. Images were acquired with an Olympus IX71 microscope (Olympus, Tokyo, Japan).

^{131}I-NGR Uptake in HT1080 Cells and HT-29 Cells

Approximately 5×10^6 CD13-positive expression HT1080 cells and CD13-negative expression HT-29 cells were seeded in a 24-well plate. After 12 hours, the culture medium was combined with ^{131}I-NGR with the activity of 0.74, 1.85, 3.70, 5.55, 7.4 MBq. After incubation for 1 hour, the culture medium was poured, the 24-well plate was washed three times with PBS, and the luminescent image was acquired.

Approximately 5×10^6, 2.5×10^6, 1.25×10^6, 6.25×10^5, and 3×10^5 CD13-positive expression HT1080 cells and CD13-negative expression HT-29 cells were seeded in a 24-well plate. After 12 hours, the culture medium was combined with ^{131}I-NGR with the activity of 7.4 MBq. After incubation for 1 hour at 37°C in a 5% CO_2 humidified air atmosphere, the culture medium was poured, the 24-well plate was washed three times with PBS, and the luminescent image was acquired. All of the experiments were performed three times.

Tumor Xenografts

All animal studies were approved by the Fourth Military Medical University (FMMU)-approved animal protocol. Female athymic nude mice ($n = 3$) were obtained from the Department of Experimental Animals (FMMU, Shaanxi, China). At 4 to 6 weeks of age, 5×10^6 HT1080 cells were injected subcutaneously in the right front flank of each mouse. When tumors reached 8 to 10 mm in diameter, the HT1080 tumor–bearing mice were subjected to in vivo imaging studies.

CLI and CLT

Na^{131}I with various activities at different depths in a tissue-mimicking phantom and various porcine tissues was acquired for the luminescent images. Both HT1080 cells and HT-29 cells combined with Na^{131}I with various activities and the two cell lines with different numbers combined with Na^{131}I were imaged with planar CLI. The mice bearing HT1080 tumors were acquired for luminescent images 8 hours after the intravenous tail injection with 22.2 MBq of ^{131}I-NGR. All of the luminescent images were acquired using the dual-modality ZKKS-Direct 3D molecular imaging system (jointly developed by Guangzhou Zhongke Kaisheng Medical Technology CO., Ltd, Xidian University, and Institute of Automation, Chinese Academy of Sciences) with a binning value of 4, integration time of 5 minutes, and aperture number of $f_{num} = 2.8$. For acquiring the biologic tissue structure, the computed tomographic (CT) images were acquired after optical imaging using the following imaging parameters: 50 kV, 1,000 µA, 480 frames, and a 5-minute scan.

The steady-state diffusion equation (DE) and Robin boundary condition can be used for describing the propagation of Cerenkov photons in biologic tissues.[21–23] Based on DE, a semiquantitative Cerenkov radiation spectral characteristic–based Cerenkov luminescent source reconstruction method was employed in this study to recover the ^{131}I-NGR distribution in living mice.[24]

In the reconstruction method, data in the entire spectra of the Cerenkov luminescent signals were used in the reconstruction of the biodistribution of the Cerenkov light source. The optical parameters of the biologic tissues over the entire spectrum were estimated based on the spectral characteristics of the Cerenkov light source and could be calculated as follows:

$$\widetilde{\mu}_a = \sum_{m=1}^{M} \rho_m \mu_a(\gamma_m) \tag{1}$$

$$\widetilde{D} = \sum_{m=1}^{M} \rho_m D(\gamma_m) \tag{2}$$

where $\widetilde{\mu}_a$ and $\widetilde{D}$ is the estimated absorption coefficient and the related diffusion coefficient in the entire spectrum of Cerenkov luminescence, respectively; M is the number of filters used for the measurement of spectrum of the emitted luminescence from the radionuclide tracer; here, $M = 4$; $\gamma_m = [\lambda_{m-1}, \lambda_m] = 1,2,...M$; and ρ_m is the percentage of optical signal intensity at M different discrete spectral ranges and can be computed by the measured spectra of the luminescence emitted from the radionuclide tracer. In this study, the estimated optical parameters of mouse adipose tissues were employed in the reconstruction process as follows: the absorption coefficient, $\mu_a \approx$

0.1017 mm^{-1}, and the reduced scattering coefficient, $\mu'_s \approx$ 1.2929 mm^{-1}. Details regarding the calculation of the optical parameters can be found in Hu and colleagues.[24]

Based on DE, an adaptive *hp* strategy was used in this study to recover the Cerenkov light source distribution.[25] Based on this method, the relationship between the Cerenkov light source and surface flux density can be established as follows:

$$\widetilde{H}_j C_j^q = \widetilde{\Psi}_j^A \quad (3)$$

where $\widetilde{H}_j$ is the system matrix for the *j*-th level mesh, which is related to the estimated optical properties; C_j^q denotes the Cerenkov light source distribution located in the permissible source region that is determined by a priori knowledge; and $\widetilde{\Psi}_j^A$ represents the nodal flux density on the mouse surface obtained without any filters.

It is difficult to solve equation 3 directly because of the ill-posed nature of the internal source reconstruction. We can employ the classic Tikhonov regularization method to solve equation 3. The following optimization problem is defined to determine the radionuclide tracer distribution:

$$\min_{C_{\inf} \leq C_j^q \leq C_{\sup}} \Theta(C_j^q) = \left\| \widetilde{H}_j C_j^q - \widetilde{\Psi}_j^A \right\|_{L^2(\Omega)} + \lambda_j \left\| C_j^q \right\|_{L^2(\Omega)} (4)$$

where C_{inf} and C_{sup} are the lower and upper bounds of the Cerenkov light source power density and λ_j represents the regularization parameter. $L^2(\Omega)$ denotes the weight matrix and satisfies $\|V\|_{L^2(\Omega)} = V^T L^2(\Omega) V$. The minimization problem is solved by use of a modified Newton method with an active set strategy.[26]

To quantify ^{131}I-NGR uptake in vivo in living mice, the CCD camera was calibrated using an integrating sphere 12 inches in diameter (USS-1200V-LL Low-Light Uniform Source, Labsphere, North Sutton, NH). The calibrated method is described in the literature.[27] Our previous study suggested that there was a linear relationship between the reconstructed power and the activity of the radionuclide-labeled probe (y = 4.56574E−5*x). Therefore, the 3D biodistribution and activity of the radionuclide labeled probe in living mice can be reconstructed.

Results

Penetration Depth Increased with Increasing Activity of Na^{131}I in the Tissue-Mimicking Phantom

For Na^{131}I with the activity of 0.037 to 0.074 MBq, the penetration depth was approximately 1 mm; for 0.185 to 2.96 MBq, it was 4 mm; for 3.7 to 18.5 MBq, it was 7 mm; and for 24.05 MBq, it was 10 mm. The data suggested that the penetration depth increased with increasing activity of Na^{131}I. The luminescent images for Na^{131}I with the activity of 3.7 MBq at a depth of 7 mm and 24.05 MBq at a depth of 10 mm are shown in Figure 1C. Additionally, we found that 0.037 MBq was approximately the minimal activity that could be detected by CLI when the depth of Na^{131}I was 1 mm; at 0.185 MBq, it was 4 mm; at 3.7 MBq, it was 7 mm; and at 24.05 MBq, it was 10 mm. The approximate minimal activity exponentially increased with an increase in Na^{131}I depth (Figure 1D). The relationship between the optical density and the optical intensity is shown in Figure 1E. The results showed that the optical intensity decreased with increasing optical density (y = 3.3675E6/1.9447^x, r^2 = .9630) at the same refractive index.

Penetration Depth of Na^{131}I is Different in Various Porcine Tissues

The linear radioactive sources of Na^{131}I (n = 4) were acquired for the luminescent images (Figure 2B). Optical signal intensity increased with increasing activity, which was consistent with our previous study.[17] Na^{131}I at different depths in various porcine tissues were acquired for the luminescent images (Figure 2C). We observed that the optical signal intensity decreased with an increase in Na^{131}I depth. Additionally, the penetration depth for Na^{131}I with more activity was greater than that with much less activity. For 0.037 MBq/μL Na^{131}I, the penetration depth in muscle was 4 mm; in fat, it was 6 mm; in kidney, it was 1 mm; and in the heart, it was 3 mm. The data suggested that the penetration depth was different in various porcine tissues. Preliminary experimental results indicated that optical signals for Na^{131}I with a concentration of 0.074 MBq/μL at a depth of 6 mm could be detected by CLI.

Characterization of ^{131}I-NGR

The purity of the synthesized NGR peptide was more than 95%. The NGR peptide was labeled with ^{131}I by iodogen with a labeling yield over 95%. ^{131}I-NGR is stable, with its purity remaining 85% at room temperature in 24 hours.

Expression of CD13 in HT1080 and HT-29 Cells

To determine the cellular origin of the APN/CD13 receptor and its activity in HT1080 and HT-29 cells, the cell lines were analyzed for CD13 protein expression via

immunofluorescence. Immunofluorescence on tumor tissue slices with CD13 antibody H300 exhibited membranous APN/CD13 antigen expression in HT1080 cells (Figure 3A), and only background staining was present in HT-29 xenografts (Figure 3B).

Robust Linear Correlation between the Cerenkov Optical Signal Intensity versus Activity and the HT1080 Cell Numbers

Approximately 5×10^6 CD13-positive expression HT1080 cells and 5×10^6 CD13-negative expression HT-29 cells were combined with ^{131}I-NGR with various activities and were acquired for luminescent images (Figure 4A). Optical signals were observed in HT1080 cells, and there was almost no signal in HT-29 cells. The data showed that there was a target for the combination of CD13 expression in HT1080 cells and NGR. Moreover, the intensity of the optical signal emitted from HT1080 cells increased linearly with the increasing activity of ^{131}I-NGR (y = 57.8389 + 1.5021x, r^2 = .9860) (Figure 4B).

HT1080 cells and HT-29 cells with different cell numbers were combined with ^{131}I-NGR with the activity of 7.4 MBq, and luminescent images were acquired (Figure 4C). Optical signals were observed in HT1080 cells, and almost no optical signal was detected in HT-29 cells. Furthermore, there was a linear correlation between the signal intensity and the cell numbers (y = 61.4703 + 1.1111E–6*x, r^2 = .9691) (Figure 4D).

CLT of APN/CD13 Expression in Mice Bearing HT1080 Tumors

Figure 5A is the photograph of the mouse bearing HT1080 tumors. The Cerenkov luminescent image of the mouse bearing HT1080 tumors was acquired 8 hours after intravenous tail injection with ^{131}I-NGR with the activity of 22.2 MBq, which is in pseudocolor superimposed on the
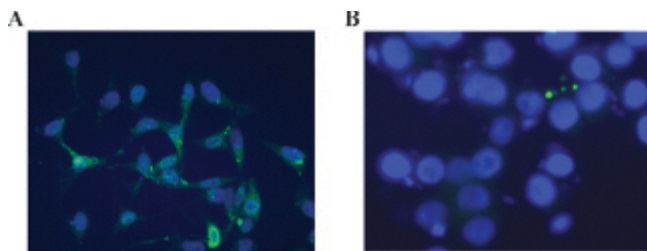

Figure 3. *A*, HT1080 cells producing high APN/CD13 levels revealed strong cellular fluorescence. *B*, HT-29 cells, which lack CD13 expression, did not bind the targeted fluorochrome (objective magnification ×40).

corresponding photograph of the mouse (Figure 5B). Luminescence was observed in the right front flanks of the mouse bearing the HT1080 tumor, indicating high expression of the APN/CD13 receptor. A few optical signals were detected in the mouse abdomen. The CT slices showed the position of the tumor obtained at z = 15.66 mm (Figure 5C) and y = 19.91 mm (Figure 5D). The green arrow represents the position of the tumor.

3D distribution of ^{131}I-NGR in the mouse tumor tissues was reconstructed using the previously described Cerenkov light source reconstruction method based on the 2D luminescent image. The 3D rendering from CLT demonstrated the 3D biodistribution and quantification of the ^{131}I-NGR in the living mouse, and the reconstructed source represented the ^{131}I-NGR uptake in the tumor tissues (Figure 5E). The 3D reconstructed CT images of the mouse showed us the position of the CT slice at z = 15.66 mm (Figure 5F). The reconstructed results clearly showed the location of the ^{131}I-NGR distributed in the right front flanks. The ^{131}I-NGR uptake in the tumor tissues represented high expression of the APN/CD13 receptor. The activity of ^{131}I-NGR uptake in the tumor of three nude mice was calculated as approximately 0.138827, 0.138819, and 0.138827 MBq, respectively. The average activity of ^{131}I-NGR uptake in the tumor was 0.1388 ± 4.6788E–6 MBq. Experimental data demonstrated the capacity of CLT for APN/CD13 expression in mice bearing HT1080 tumors.

Discussion

In vivo imaging of APN/CD13 expression is crucial for the early detection of cancer. To the best of our knowledge, we imaged the abnormal expression of APN/CD13 in tumorigenesis with the novel CLT for the first time. The reconstructed results of ^{131}I-NGR uptake in the tumor tissues demonstrated the ability of CLT to image and quantify the expression of the APN/CD13 receptor.

CLI results of the in vitro cell experiment showed that optical signals were observed clearly in HT1080 cells cultured with ^{131}I-NGR. However, little signal was observed in HT-29 cells, which was coincident with the results of immunofluorescence. Our study indicated that NGR can specifically bind with CD13 expressed in HT1080. Therefore, CLI can be used for the imaging of ^{131}I-NGR uptake in HT1080 cells. Moreover, the emitted optical signal linearly increased with increasing cell number, which suggested the potential of the CLT technique to accurately image APN/CD13 expression.
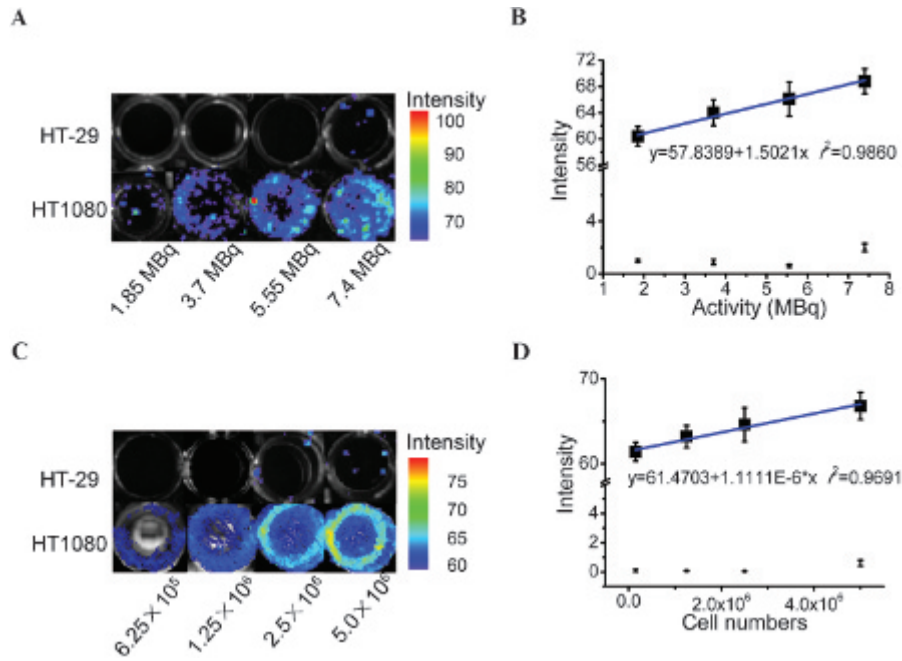
Figure 4. In vitro CLI of ^{131}I-NGR uptake in HT1080 cells and HT-29 cells. *A,* The luminescent images of 5×10^6 CD13-positive expression HT1080 cells and 5×10^6 CD13-negative expression HT-29 cells combined with ^{131}I-NGR with various activities are shown. *B,* The intensity of the optical signal emitted from HT-1080 cells increased with increasing activity of ^{131}I-NGR. *C,* The acquired luminescent images of HT1080 cells and HT-29 cells with different cell numbers combined with ^{131}I-NGR with the activity of 7.40 MBq. *D,* There was a linear correlation between the signal intensity and the cell numbers.
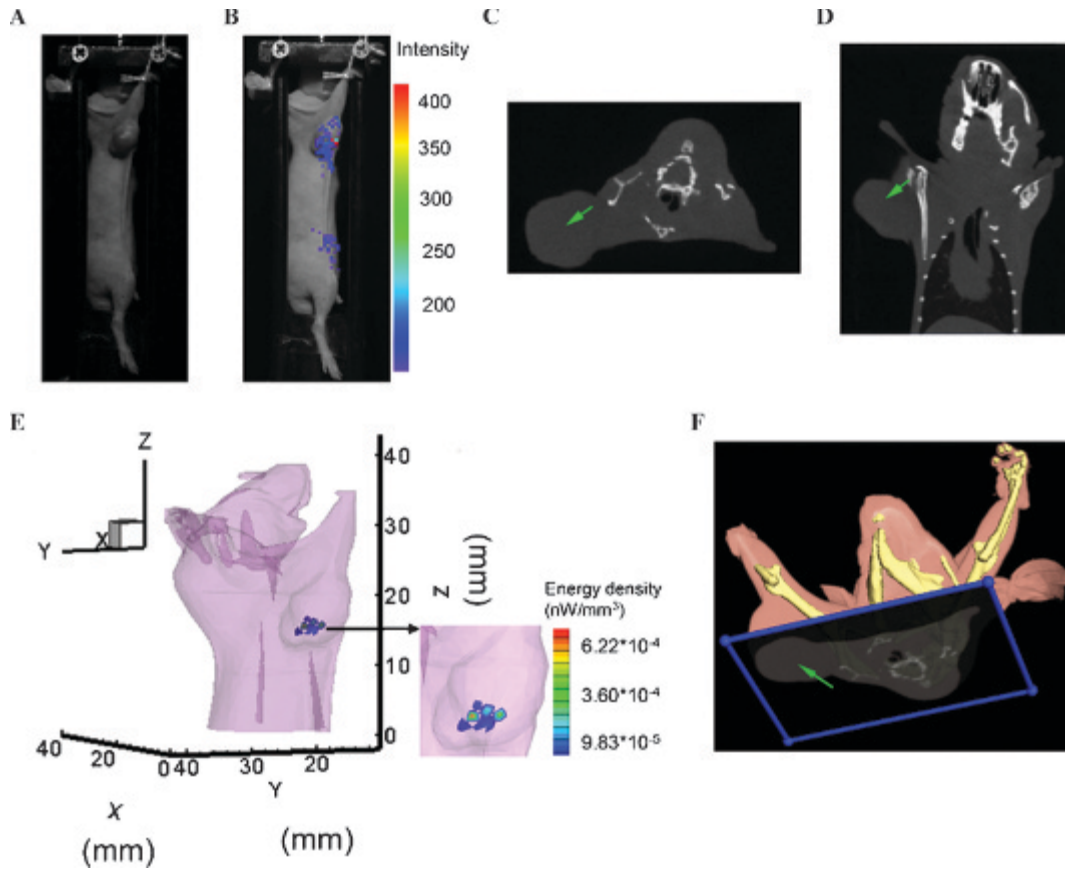
Figure 5. *A,* Photograph of the mouse bearing HT1080 tumors. *B,* Cerenkov luminescent image of the mouse bearing HT1080 tumors 8 hours after intravenous tail injection with ^{131}I-NGR with the activity of 22.2 MBq. *C,* The horizontal view of the computed tomographic (CT) results at $z = 15.66$ mm. *D,* The coronal view of the CT results at $y = 19.91$ mm. *E,* The 3D distribution of ^{131}I-NGR in the mouse bearing HT1080 tumors. The reconstructed source representing the ^{131}I-NGR uptake in the tumor tissues. *F,* The 3D reconstructed CT images of the mouse, which show the position of the CT slice at $z = 15.66$ mm. The *green arrow* represents the position of the tumor.

The experimental reconstruction of an implantation mouse model with a Na^{131}I radioactive source validated the performance of the semiquantitative hybrid spectral reconstruction method.[24] We employed the reconstruction method to reconstruct the 3D biodistribution of ^{131}I-NGR in living mice. The results indicated that ^{131}I-NGR uptake in the tumor tissues represented high expression of the APN/CD13 receptor. The average activity of ^{131}I-NGR uptake in the tumor tissues was reconstructed as 0.1388 ± 4.6788E–6 MBq. It was notable that unlike with 2D planar CLI, we could obtain the location and quantification information of a radionuclide-labeled probe using the 3D CLT technique, which is significant for the diagnosis and treatment of cancer.

The main disadvantage of CLI is limited penetration. We investigated the penetration of Cerenkov luminescence emitted from ^{131}I using the tissue-mimicking phantom and various porcine tissues. Our preliminary data indicated that the penetration depth increased with increasing activity of Na^{131}I, and Cerenkov luminescence could penetrate the shallow porcine tissue. The maximal activity used in the experiment was 24.05 MBq. The activity of the radiopharmaceutical used in clinics is usually 12 mCi. Therefore, it was possible for CLI/CLT to be applied in the imaging of shallow tissues in clinics.

CLT provides a new avenue for the imaging of APN/CD13 expression. Compared to nuclear imaging and FMT, CLT has many advantages, such as being an inexpensive optical instrument and having high throughput, high resolution, and no problems with probe toxicity. Moreover, based on Cerenkov radiation, the radionuclide-labeled probe can also be imaged via the optical imaging system. The inherited multimodality imaging of combining optical and nuclear imaging can easily be achieved with a single radioisotope or radionuclide-labeled probe. Thus, CLT has the potential for imaging APN/CD13 expression and potentially promotes the application of a novel optical imaging technique in the early detection of cancer. Additionally, this promising technique could be potentially used for evaluating tumor response to chemotherapy or radiotherapy.

Conclusion

In this study, we imaged the abnormal expression of APN/CD13 in mice bearing HT1080 tumors with novel CLT. The reconstructed results of ^{131}I-NGR uptake in the tumor tissues demonstrated the ability of CLT to image and quantify the expression of the APN/CD13 receptor. Our study indicated that this promising technique could

potentially be used for sensitively evaluating tumor angiogenesis in vivo.

References

1. Folkman J. Tumor angiogenesis: therapeutic implications. N Engl J Med 1971;285:1182–6, doi:10.1056/NEJM197108122850711.
2. Folkman J. Angiogenesis in cancer, vascular, rheumatoid and other disease. Nat Med 1995;1:27–31, doi:10.1038/nm0195-27.
3. Wickstrom M, Larsson R, Nygren P, et al. Aminopeptidase N (CD13) as a target for cancer chemotherapy. Cancer Sci 2011;102:501–8, doi:10.1111/j.1349-7006.2010.01826.x.
4. Wang R, Niu Y, Wu H, et al. Development of NGR peptide-based agents for tumor imaging. Am J Nucl Med Mol Imaging 2011;1:36–46.
5. von Wallbrunn J, Waldeck J, Holtke C, et al. *In vivo* optical imaging of CD13/APN-expression in tumor xenografts. J Biomed Opt 2008;13:011007–1–9, doi:10.1117/1.2839046.
6. Robertson R, Germanos MS, Li C. Optical imaging of Cerenkov light generation from positron-emitting radiotracers. Phys Med Biol 2009;54:355–65, doi:10.1088/0031-9155/54/16/N01.
7. Spinelli AE, D'Ambrosio D, Calderan L, et al. Cerenkov radiation allows *in vivo* optical imaging of positron emitting radiotracers. Phys Med Biol 2010;55:483–95, doi:10.1088/0031-9155/55/2/010.
8. Liu H, Ren G, Miao Z, et al. Molecular optical imaging with radioactive probes. Plos One 2010;5:e9470, doi:10.1371/journal.pone.0009470.
9. Boschi F, Spinelli AE, D'Ambrosio D, et al. Combined optical and single photon emission imaging: preliminary results. Phys Med Biol 2009;54:L57–62, doi:10.1088/0031-9155/54/23/L01.
10. Boschi F, Calderan L, D'Ambrosio D, et al. In vivo ^{18}F-FDG tumour uptake measurements in small animals using Cerenkov radiation. Eur J Nucl Med Mol Imaging 2011;38:120–7, doi:10.1007/s00259-010-1630-y.
11. Ruggiero A, Holland JP, Lewis JS, et al. Cerenkov luminescence imaging of medical isotopes. J Nucl Med 2010;51:1123–30, doi:10.2967/jnumed.110.076521.

12. Dothager RS, Goiffon RJ, Jackson E, et al. Cerenkov radiation energy transfer (CRET) imaging: a novel method for optical imaging of PET isotopes in biological systems. Plos One 2010;5: e13300, doi:10.1371/journal.pone.0013300.

13. Spinelli AE, Meo SL, Calandrino R, et al. Optical imaging of Tc-99m-based tracers: in vitro and in vivo results. J Biomed Opt 2011; 16:116023, doi:10.1117/1.3653963.

14. Holland JP, Normand G, Ruggiero A, et al. Intraoperative imaging of positron emission tomographic radiotracers using Cerenkov luminescence emissions. Mol Imaging 2011;10:177–86.

15. Mitchell GS, Gill RK, Boucher DL, et al. In vivo Cerenkov luminescence imaging: a new tool for molecular imaging. Philos Trans R Soc A 2011;369:4605–19, doi:10.1098/rsta. 2011.0271.

16. Li C, Mitchell GS, Cherry SR. Cerenkov luminescence tomography for small animal imaging. Opt Lett 2010;35:1109–11, doi:10.1364/OL.35.001109.

17. Hu Z, Liang J, Yang W, et al. Experimental Cerenkov luminescence tomography of the mouse model with SPECT imaging validation. Opt Express 2010;18:24441–50, doi:10.1364/OE.18.024441.

18. Spinelli E, Kuo C, Rice BW, et al. Multispectral Cerenkov luminescence tomography for small animal optical imaging. Opt Express 2011;19:12605, doi:10.1364/OE.19.012605.

19. Wang G, Li Y, Jiang M. Uniqueness theorems in bioluminescence tomography. Med Phys 2004;31:2289–99, doi:10.1118/1. 1766420.

20. Alexandrakis G, Rannou FR, Chatziioannou AF. Tomographic bioluminescence imaging by use of a combined optical-PET

21. (OPET) system: a computer simulation feasibility study. Phys Med Biol 2005;50:4225, doi:10.1088/0031-9155/50/17/021.

21. Farrell TJ, Patterson MS, Wilson B. A diffusion theory model of spatially resolved, steady-state diffuse reflectance for the non-invasive determination of tissue optical properties in vivo. Med Phys 1992;19:879–88, doi:10.1118/1.596777.

22. Gurfinkel M, Pan TS, Sevick-Muraca EM. Determination of optical properties in semi-infinite turbid media using imaging measurements of frequency-domain photon migration obtained with an intensified charge-coupled device. J Biomed Opt 2004;9:1336–46, doi:10.1117/1.1803549.

23. Schweiger M, Arridge SR, Hiraoka M, et al. The finite element method for the propagation of light in scattering media: boundary and source conditions. Med Phys 1995;22:1779–92, doi:10.1118/1.597634.

24. Hu Z, Ma X, Qu X, et al. Three-dimensional noninvasive monitoring iodine-131 uptake in the thyroid using a modified Cerenkov luminescence tomography approach. PLoS One 2012;7: e37623, doi:10.1371/journal.pone.0037623.

25. Han R, Liang J, Qu X, et al. A source reconstruction algorithm based on adaptive *hp*-FEM for bioluminescence tomography. Opt Express 2009;17:14481–94, doi:10.1364/OE.17.014481.

26. Gill PE, Murray W, Wright M. Practical optimization. New York: Academic Press; 1981.

27. Liu J, Chen D, Li X, et al. In vivo quantitative reconstruction studies of bioluminescence tomography: effects of peak wavelength shift and model deviation. IEEE Trans Biomed Eng 2010;57:2579–82, doi:10.1109/TBME.2010.2056370.